Separation Science and Technology
Publication details, including instructions for authors and subscription information:
http://www.informaworld.com/smpp/title~content=t713708471

Fabrication and Vapor-Phase Adsorption Characterization of Acetone and *n*-Hexane onto Carbon Nanofibers

Chien-Te Hsieh[a]; Yun Wen Chou[a]
[a] Department of Chemical Engineering and Materials Science, Fuel Cell Center, Yuan Ze University, Taiwan, Republic of China

To cite this Article Hsieh, Chien-Te and Chou, Yun Wen(2006) 'Fabrication and Vapor-Phase Adsorption Characterization of Acetone and *n*-Hexane onto Carbon Nanofibers', Separation Science and Technology, 41: 14, 3155 — 3168
To link to this Article: DOI: 10.1080/01496390600854594
URL: http://dx.doi.org/10.1080/01496390600854594

Separation Science and Technology, 41: 3155–3168, 2006

ISSN 0149-6395 print/1520-5754 online
DOI: 10.1080/01496390600854594

Fabrication and Vapor-Phase Adsorption Characterization of Acetone and *n*-Hexane onto Carbon Nanofibers

Chien-Te Hsieh and Yun Wen Chou
Department of Chemical Engineering and Materials Science,
Fuel Cell Center, Yuan Ze University, Taiwan, Republic of China

Abstract: Vapor-phase adsorption of acetone and *n*-hexane by different carbon nanofibers (CNFs) was investigated. Two kinds of CNFs with different pore size distributions were fabricated by the two syntheses: thermal chemical vapor deposition and template-assisted synthesis. Langmuir and Dubinin-Radushkevich models were employed to estimate the surface accessibility to adsorbates and the mean energy during the adsorption. It was suggested on the basis of the present work that the surface area and micropore fraction of the CNFs are important factors in determining the adsorption capacity. Both the equilibrium constant and free energy for adsorption are favorable for the CNFs with the mesopore fraction, indicating that the presence of mesopores facilitates the adsorption to high-energy sites.

Keywords: Carbon nanofibers, vapor-phase adsorption, volatile organic compounds, template synthesis, pore structures

INTRODUCTION

Since the discovery of carbon nanotubes (CNTs) by Iijima (1), such one-dimensional nanomaterials have attracted much attention in a variety of applications such as separation, gas sensing, catalyst support, energy storage, and environmental protection (2, 3). Numerous studies (4–7) have devoted

Received 21 February 2006, Accepted 16 May 2006
Address correspondence to Chien-Te Hsieh, Department of Chemical Engineering and Materials Science, Fuel Cell Center, Yuan Ze University, Taoyuan 320, Taiwan, Republic of China. Tel.: + 886-3-4638800 ext. 2577; Fax: +886-3-4559373; E-mail: cthsieh@saturn.yzu.edu.tw

to synthesizing various CNT or carbon nanofiber (CNF) products by using arc discharge, chemical vapor deposition (CVD), plasma-assisted CVD approaches, and so on. Up to now, the CVD method is still one of popular syntheses because of its scale-up capability. Using the method, CNFs are easily produced by the catalytic decomposition of certain hydrocarbons on small metal particles, such as Ni, Fe, and other metal oxides. A pioneer study (6) has pointed out that the diameter of the as-grown nanotubes are significantly controlled by the catalyst size. This finding reflects that the desired diameter of CNFs can be prepared when the size of the catalyst is well controlled. However, the fabrication of well-ordered CNT arrays is still a challenge, which may require a great effort in depositing uniform catalysts by using advanced techniques, e.g., electron beam combined with lithography. Recently, template synthesis for preparing ceramic or oxide nanofibers, such as SnO_2, ZnO, and SiO_2, has gradually emerged in literature (8–10). Usually, a porous membrane made from anodic alumina oxide (AAO) or polymer is employed as a template that has a large quantity of nano-channels. The uniform open-tipped structure can confine to a desired outer diameter of the nanofibers. Thus, this approach is suitable for synthesizing well-defined CNFs (11).

In general, these nanotubes consist of rolled-up graphene sheets that can be divided into single-walled nanotubes (SWNTs) and multi-walled nanotubes (MWNTs) depending on their synthesis methods (3). The CNTs have inner hollow cavities with diameters typically ranging from 5 to 50 nm, which is beneficial for adsorbing or separating molecules from the gaseous or the aqueous phase. Thus, the CNTs/CNFs gradually become a promising candidate that can serve as an effective adsorbent of atoms and molecules (3, 11–16). For example, Eswaramoorthy et al. have investigated the adsorption of benzene and methanol in SWNTs that revealed type II adsorption isotherms with an uptake of 100–300 mg/g (12). In 2003, Li et al. indicated that CNTs possess a high Pb^{2+} adsorption capacity ($\sim$97.1 mg/g), capable of removing heavy metal ions from water (3). After that, this group reported that CNTs are good fluoride adsorbents and their removal capability exceeds commercial activated carbon (13). Cinke et al. developed a high-pressure CO disproportionation process to synthesize high-surface area SWNTs (Brunauer-Emett-Teller (BET) surface area: 1587 m^2/g) that can adsorb nearly twice the volume of CO_2 compared to activated carbon (14). Peng et al. explored that CNTs shows good removal ability for separating 1,2-dichlorobenzene from water in a wide pH range of 3–10 (16). Our previous study (11) has indicated that CNF array prepared by a template-based method has a higher *n*-hexane adsorption capacity and can rapidly achieve an equilibrium coverage. More recently, Lu et al. showed that MWNTs have a high adsorption capacity for trihalomethanes removal in liquid phase (16).

According to the literatures mentioned above, CNTs/CNFs exhibit a potential as high-performance adsorbents for physisorption of various adsorbates in gaseous or aqueous phase. This probably directs us to develop a novel gas-storage device, high-sensitivity gas sensor, separation membrane,

and so on. To achieve further applications, an understanding of the adsorption behavior of common adsorbates in CNFs is required. The major interest of this study is to investigate volatile organic compounds' (VOCs) adsorption on different CNFs at ambient temperature in vapor phase. In this work, two types of CNFs were fabricated by template-based and catalytic hydrocarbon decomposition synthesis, respectively. Adsorptions of VOCs, acetone, and *n*-hexane, from gaseous phase were conducted to characterize the carbon adsorbers. A series of adsorption experiments were carried out and the resulting adsorption isotherms were interpreted by using well-developed models including Langmuir and Dubinin-Radushkevich (DR) models.

EXPERIMENTAL PROCEDURE

A template-assisted technique using epoxy/toluene as a carbon precursor to produce aligned CNFs arrays has been reported elsewhere (11). The as-grown CNFs with heights of 50 μm and diameters of 100 nm can be conveniently controlled with ordered and vertical walls. The template synthesis can be summarized in the following three steps. Firstly, an epoxy resin/toluene (1:2 in v/v) solution is introduced into an anodic alumina oxide (AAO) template that has a high nanochannel density ($10^9/cm^2$) with an average pore diameter of 100 nm. The size and the thickness of the AAO template is about $1 \times 1\ cm^2$ and 50 μm, respectively. Next, the prepared template is carbonized at 700°C under an Ar atmosphere. This carbonization process enables the solidification of aligned CNFs along the vertical direction via template assistance. Finally, 3 M KOH chemical etching is employed to remove the template, thus leaving the ordered CNFs array exposed. The diameter and real density of hollow nanofibers are controlled by the morphologies of the AAO template.

A simplified thermal chemical vapor deposition (CVD) was employed to grow the other type of CNFs in this present work. At first, 0.5 M nickelous nitrate ($Ni(NO_3)_2 \cdot 6H_2O$) solution was prepared as a catalyst precursor, then the as-received solution was uniformly covered onto the stainless foil by spin-coating. For easy control of the quantity of metal particle on the substrate, we fixed the rotational speed of the spin center at 1200 rpm. The derived substrate was dried in a vacuum oven at 350°C for 1 h for nitrate decomposition and subsequent cooling, both in Ar, to give the Ni-impregnated catalyst. Here the thermal growth process was performed in a rectangle reactor installed in an electrical furnace, using a mixture vapor (toluene/Ar) as a carbon precursor. The growth process was carried out at the desired temperature of 900°C for 1 h and kept at a pressure of 1 atm. To remove the catalyst particles, the grown CNFs were acid-washed (1 M nitric acid) under an ultrasonic bath. The purification procedure was performed for 2 h, and then the resulting dispersion was filtered and rinsed twice with deionized water. Finally, the CNFs were dried at 110°C in a vacuum oven overnight. The morphology of the CNFs was

observed by field-emission scanning electron microscopy (FE-SEM, LEO 1530) and transmission electron microscopy (TEM, JEOL 2010).

Porous characterizations of the CNFs were determined by N_2 adsorption at $-196^{\circ}C$, using an automated adsorption apparatus (Micromeritics ASAP 2010). Specific surface areas and porosities of these carbons were determined by gas adsorption. Before any such analysis the sample was degassed at $300^{\circ}C$ in a vacuum at about 10^{-3} Torr. Surface areas and micropore volumes of the samples were determined from the application of the BET and DR equations, respectively, to the N_2 adsorption isotherms at relative pressures between 0.06 and 0.2. The amount of N_2 adsorbed at relative pressures near unity ($P/P_0 = 0.98$ here) corresponds to the total amount adsorbed at both micropores and mesopores. The *t*-plot (17, 18) was employed in estimating the total surface area (S_t). The density functional theory (DFT) (19, 20) method was used to analyze pore size distribution (0.5 to 1000 nm), respectively.

A standard thermogravimetric analyzer, TGA (Perkin-Elmer TA7) was used for gaseous-adsorption experiments of CNFs. Prior to the adsorption experiment, the carbon surface was cleaned of oxides by heating the sample to $500^{\circ}C$ in extra-purity helium for 0.5 h. The experiments of adsorption were performed after surface cleaning by lowering the temperature of the sample to the desired adsorption temperature, and then quickly introducing the desired VOC/He mixture. The adsorption temperature was set at $30^{\circ}C$, and the gas flow of VOC/He gas was at 100 cm^3/min. Mass uptake of the VOCs during adsorptive experiments was continuously monitored for at least 2 h, at which the rate of mass gain was negligible.

RESULTS AND DISCUSSION

Surface Characteristics of the Resulting CNFs

To distinguish the as-grown CNFs, two kinds of the CNFs are denominated as CNF-T (template-assisted synthesis) and CNF-C (catalytic hydrocarbon decomposition), respectively. Figures 1(a) and 1(b) illustrate FE-SEM images of the CNF arrays, showing an obvious difference between CNF-T and CNF-C in morphology. A well-ordered CNF-T looks like a bundle of open-tipped tubules while coiled CNF-C has a disorder array grown on stainless substrate. The typical bright-field TEM images of single CNF-T and CNF-C are shown in Figs. 1(c) and 1(d), respectively. We observe that both of the CNFs have smooth outer surfaces, and the inner surfaces of the nanofibers look hollow and rough. The aligned CNF-T has the form of tubules with an outer diameter of $\sim$100 nm and a length of $\sim$50 μm, indicating that the growth of CNF-T is well confined within the pore of the AAO template. Otherwise, the length and the outer diameter of the individual CNF-C is about 10–20 μm and 50–100 nm, respectively.

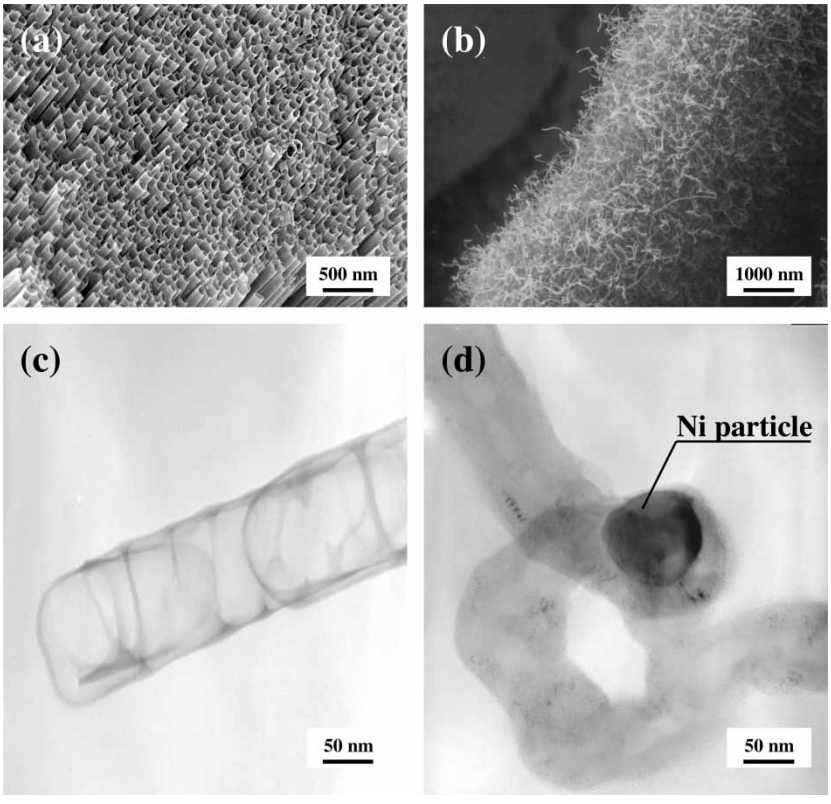

Figure 1. FE-SEM photographs of the carbon nanofibers: (a) CNF-T and (b) CNF-C. HR-TEM images of the carbon nanofibers: (c) CNF-T and (d) CNF-C.

Nitrogen physisorption on porous media has been widely applied in determining the pore structures, including the BET surface area, pore volume, and pore size distribution (PSD) (21). It has to emphasize the limit of pore size for micropore (pore size: <2 nm) and mesopore (pore size: 2–50 nm). The adsorption and desorption isotherms of N_2 on the CNFs are shown in Fig. 2. These isotherms have a rounded knee at low relative pressure indicating a micropore volume in the CNFs, a plateau with a sharp slop suggesting a mesoporous surface area, an adsorption "tail" at high pressure, and a desorption hysteresis loop due to nitrogen condensation in mesopores, i.e., typically a type II isotherm (21). It is clear that CNF-T has a larger N_2 adsorption capacity than CNF-C, reflecting a larger amount of porosity in CNF-T.

The surface characteristics of CNFs determined from N_2 isotherms are given in Table 1. As shown in Table 1, CNF-T has a greater specific surface area, total pore volume, and mesopore fraction than CNF-C. Their

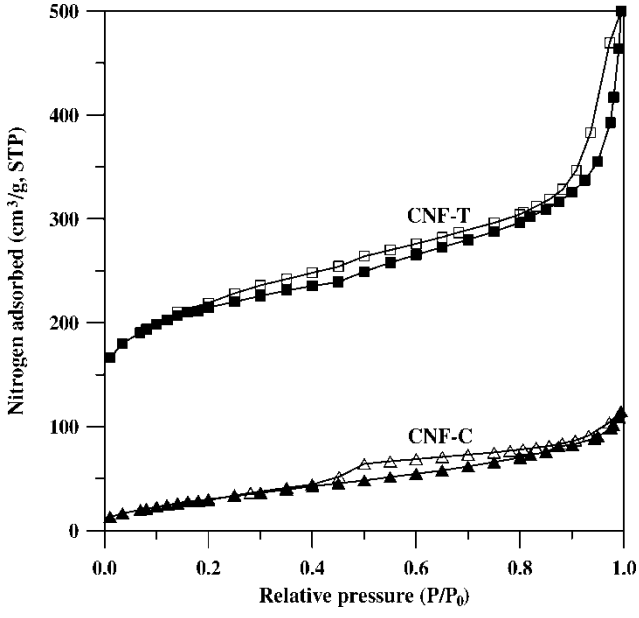

Figure 2. Adsorption (solid symbol) and desorption (empty symbol) isotherms of N_2 onto the carbon nanofibers at −196°C.

results are in agreement with the observations from Fig. 2. The detailed PSDs of CNFs were calculated by employing the regularization method according to the density functional theory (DFT), which is based on a molecular model for adsorption of nitrogen in porous solids (13). Figure 3 shows that both of the CNFs have mainly a mesoporous structure, which is identical with the observation in Fig. 2. It is observed from Fig. 3 that CNF-T possesses a broader PSD with bimodal or trimodel including microporous and mesoporous

Table 1. Surface characteristics of carbon nanofibers by different synthesis methods

	Specific surface area (m^2/g)		Pore volume (cm^3/g)		
Carbon type	S_{BET}[a]	S_t[b]	V_t[c]	V_{micro}[d] (%)	V_{meso}[e] (%)
CNF-T	780	795	0.66	0.13(20)	0.53(80)
CNF-C	121	125	0.16	0.04(39)	0.12(61)

[a]S_{BET}: specific surface area computed using BET equation.
[b]S_t: specific surface area determined by *t*-plot method.
[c]V_t: total pore volume estimated at a relative pressure of 0.98.
[d]V_{micro}: micropore volume determined from the Dubinin-Radushkevish equation.
[e]V_{meso}: mesopore volume determined from the subtraction of micropore volume from total pore volume.

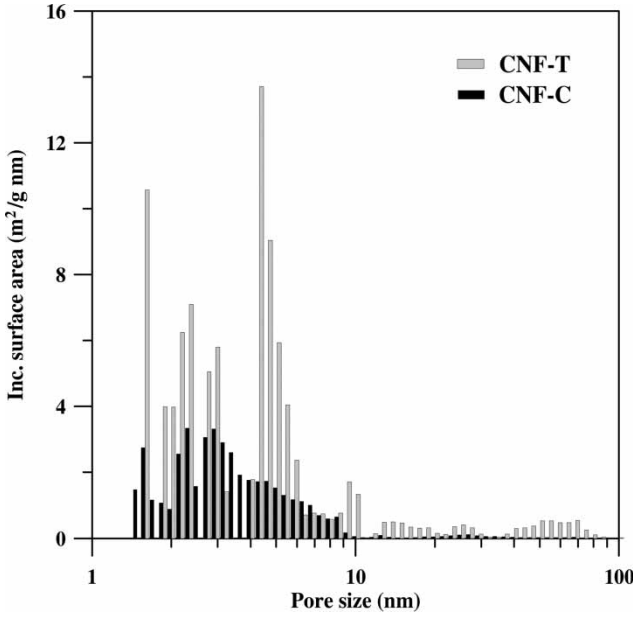

Figure 3. Pore size distributions of the carbon nanofibers determined from the DFT model.

size (1.4–50 nm), while the PSD of CNF-C is concentrated at the pore size range of 1.4–10 nm. We infer that the main porosity in the CNFs is contributed by the inter-aggregate voids in hollow fibers and the interspaces among each of the fibers.

Data Interpretation with Langmuir Isotherm Model

Figures 4 and 5 show the equilibrium adsorption isotherms of acetone and *n*-hexane, respectively, onto different CNFs in the vapor phase. The typical isotherms represent a relationship between the VOCs adsorbed per unit weight of the carbon adsorbers and their vapor pressure in gas phases. As expected, the adsorption capacities of CNF-T are greater than that of CNF-C for both VOCs. This is presumably due to the fact that CNF-T has a high BET-surface area that is six times higher than CNF-C. This trend is reasonable because the surface area of adsorbents is an important factor determining the adsorption capacities of the adsorbents (22). As observed in these isotherms, the shape of the isotherms is of the Langmuir-type, in which the isotherms show the trend of leveling out at higher adsorbate concentrations, corresponding to the completion of a monolayer in the experimental concentration range (23).

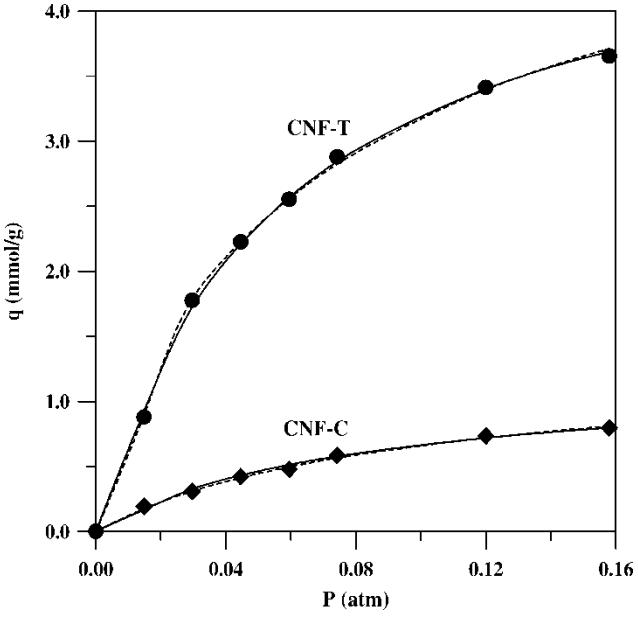

Figure 4. Adsorption isotherms of acetone on the carbon nanofibers at 30°C. In this figure, the symbols are experimental data, and the solid and dashed line curves are simulated from the Langmuir and DR equations, respectively.

Adsorption isotherms are important to describe how adsorbates will interact with carbon and are critical in optimizing the use of carbon as an adsorber. Thus, the correlation of equilibrium data using either a theoretical or empirical equation is essential to practical adsorption operation. Although the adsorption mechanism of CNFs in vapor phase is complicated in nature, the correlation of equilibrium data with a theoretical equation giving a satisfactory description of the adsorption is looked upon as offering a clue to the key mechanistic steps in the overall adsorption process. Two famous two-parameter isotherm equations, Langmuir and DR, were employed for further interpretation of the adsorption data obtained in the preceding section.

The most widely employed two-parameter equation is the Langmuir equation, which is represented as

$$q_e/q_m = (K_L P)/(1 + K_L P) \tag{1}$$

where q_e is the amount of VOCs adsorbed on CNFs at a partial pressure P, q_m is the adsorption capacity corresponding to complete monolayer coverage, and K_L is the Langmuir constant, which can be considered as a measure of adsorption energy (24). A linear plot of (P/q_e) against P would give q_m and K_L from the slope and intercept, respectively. These parameters, together with the correlation coefficient (r^2), of the Langmuir equation for the adsorption

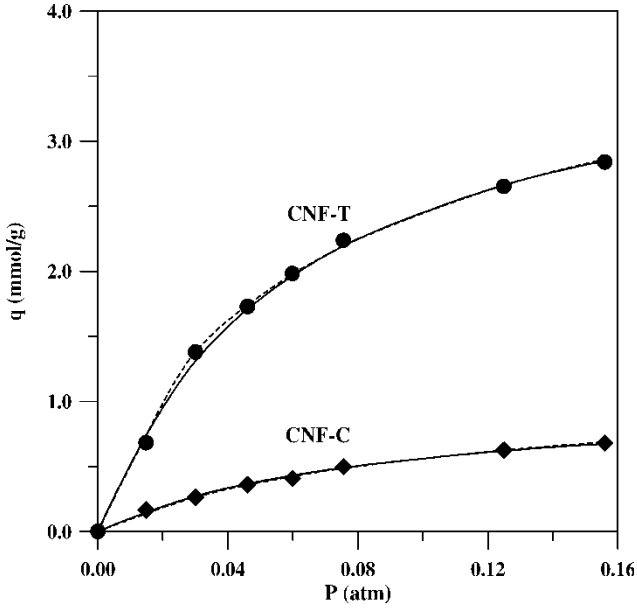

Figure 5. Adsorption isotherms of *n*-hexane on the carbon nanofibers at 30°C. In this figure, the symbols are experimental data, and the solid and dashed line curves are simulated from the Langmuir and DR equations, respectively.

of acetone and *n*-hexane onto different CNFs are shown in Table 2. The Langmuir equation gives fairly good fits to the acetone and *n*-hexane isotherms ($r^2 > 0.983$). As expected from the results of Figs. 4 and 5, the monolayer adsorption capacities (q_m) for both acetone and *n*-hexane increase with the increasing surface area of the CNFs.

It is of interest that the capacity of the CNFs does not show a proportional increase with the increasing surface area. This finding can be supported by the fact that the total surfaces or porosities of the CNFs

Table 2. Parameters of Langmuir adsorption isotherms for acetone and *n*-hexane adsorption onto carbon nanofibers at 30°C

Carbon type	q_m (mmol/g)	K_L (1/atm)	r^2	M_L (μmol/m^2)
Acetone adsorption				
CNF-T	5.00	17.7	0.998	6.41
CNF-C	1.19	12.7	0.981	9.83
n-Hexane adsorption				
CNF-T	3.95	16.5	0.996	5.06
CNF-C	1.04	11.9	0.986	8.60

cannot be fully accessed by VOC molecules and do not have a uniform distribution of the adsorptive sites. To realize the active surface for the VOC adsorption, a surface accessibility of the CNFs to acetone and *n*-hexane was examined, by calculating the maximum proportion of the BET surface area that can be occupied by the adsorbates. Theoretically, the value of q_m represents the limiting number of sites that are capable of adsorbing adsorbates. Thus, the M_L values that represent the maximum fraction of the BET area covered by the adsorbates can be estimated according to q_m. The values of M_L are also listed in Table 2. The results show that for the adsorption of both acetone and *n*-hexane, the M_L values of CNF-C exceeds that of CNF-T, implying that the adsorptive accessibility is affected by the pore structures. Since adsorption of many VOCs in micropores of carbonaceous solids has been mainly attributed to the dispersion force (25), the size of the micropore is therefore playing a major role in the attraction of adsorbate molecules. In the adsorption process, it is generally believed that micropores are the major provider of adsorption sites, whereas in mesopores only weaker adsorption is observed (26). This clearly shows that the affinity of the carbon surface to adsorbates, i.e., the energy for adsorption has an inverse trend with the pore size of the adsorbent. As analyzed by the DFT model (Fig. 3), this can be attributed to the fact that CNF-C possesses a narrower PSD than CNF-T, thus facilitating a greater accessibility for VOC adsorption on CNF-C.

The data in Table 2 show that the Langmuir constant (K_L) of CNF-T has a higher value than that of CNF-C. Theoretically, the K_L represents the equilibrium constant of an idealized adsorption process expressed in thermodynamic terms as

$$C^* + A \longleftrightarrow C^*(A) \quad (R1)$$

where A is the adsorbate molecule in vapor phase, C^* the available adsorptive site of the CNFs, and $C^*(A)$ the site occupied by adsorbate. The sum of the numbers of C^* and $C^*(A)$ is the total number of the adsorbing sites, which is equivalent to the value of q_m. A larger value in the equilibrium constant (K_L) indicates a stronger adsorption on the adsorptive site. The K_L value of CNF-T reflects that the mesoporous structure fabricated by the template-assisted method would result in a higher adsorption intensity for the adsorptive sites, although the fraction of the surface accessible to the adsorbates was found to have a lower value. The K_L value might thus be attributed to the existence of mesopores that is probably contributed by the bundle of nanofibers and the inner diameter of the individual nanofiber. Therefore, this unique pore structure facilitates the adsorption of the adsorbates onto interior sites, which have stronger binding energies. This explanation can be supported by the analysis using the DR model presented later in this paper.

Data Interpretation with DR Isotherm Model

The adsorption data can be further interpreted by the DR equation (27). In deriving this equation for gaseous-phase adsorption, the amount adsorbed corresponding to any partial pressure of VOCs is assumed to be a Gaussian function of the Polanyi potential (28), ε,

$$q_e = q_{DR} \exp(B\varepsilon^2) \tag{2}$$

with

$$\varepsilon = RT \ln(P_0/P) \tag{3}$$

where q_{DR} is the maximum amount of adsorbate in the CNFs, B is a constant related to the energy, and P/P_0 is the partial pressure. If the carbon surface is heterogeneous and an approximation to a Langmuir isotherm is chosen as the local isotherm on each homogeneous subregion (29), then the most probable free energy of adsorption is

$$E = (2B)^{-1/2} \tag{4}$$

Therefore, the use of the DR equation results in an estimation of the maximum adsorption capacity as well as an average free energy value unique to the adsorbate-adsorbent system. The DR equation can be linearized as

$$\ln q_e = \ln q_{DR} - B\varepsilon^2 \tag{5}$$

A linear plot of $\ln q_e$ against ε^2 would give the values of q_{DR} and B (thus the mean free energy of adsorption, E) from the intercept and slope, respectively. The parameters of the DR equation for the adsorption of acetone and *n*-hexane were determined, as shown in Table 3. The correlation factors (r^2) are also listed in the table, showing that the linear fit is fairly good for the adsorption of all the adsorbates.

As expected, the values of the maximum adsorption capacities (q_{DR}) determined by the DR equation are found to have an order of

Table 3. Parameters of dubinin-radushkevich adsorption isotherms for acetone and *n*-hexane adsorption onto carbon nanofibers at 30°C

Carbon type	q_{DR} (mmol/g)	E (kJ/mol)	r^2	M_{DR} (μmol/m^2)
Acetone adsorption				
CNF-T	4.90	6.13	0.998	6.28
CNF-C	1.17	5.35	0.994	9.69
n-Hexane adsorption				
CNF-T	3.80	6.10	0.991	4.87
CNF-C	1.00	5.32	0.997	8.26

CNF-T > CNF-C, which is identical to those of BET surface area and q_m. To estimate the accessibility of each adsorbate to the surface of the CNFs, the values of q_{DR} were divided by the BET surfaces of the adsorbents to give the maximum surface available for the adsorption, which was designated as M_{DR}. The values of M_{DR} for the adsorption of the CNFs are also been listed in Table 3. Similar to the findings from the Langmuir analysis in evaluating M_L, Table 3 shows that the M_{DR} values of CNF-C are higher than that of CNF-T for both adsorbates, reflecting again that the micropores in the CNFs may play a major in adsorbing VOC molecules.

It is of interest that the values of M_{DR} are slightly smaller than those of M_L for the adsorption of both acetone and *n*-hexane. This difference in the fraction of coverage reflects that the assumption of monolayer adsorption in the Langmuir model may result in the underestimation of the ultimate adsorption capacity of the CNFs. Furthermore, it is very likely that the Langmuir analysis underestimates the adsorption energy. In the Langmuir model, the carbon surface is assumed to be homogeneous and a single energy applies to all adsorption sites. The average energy determined by Langmuir analysis would be approximately the same as the isosteric heat of adsorption estimated near the completion of surface coverage (30). Because the higher energy sites are covered initially, the heat estimated near the full coverage actually represents the minimum value of the site energies. Underestimation of the site energy would probably be one of the reasons causing the underestimation of the ultimate adsorption capacity in the Langmuir model.

The mean free energy (E) determined from the DR equation is related to the pore size of the porous system (31). Table 3 shows that for both adsorbates, CNF-T has a greater value of E than CNF-C, demonstrating again that mesopores enable the adsorbates to get access to the inner and narrow micropores, where the pore walls provide overlapping potentials to increase the free energy for adsorption (32). This finding is in agreement with the preceding interpretation that the existence of mesopores facilitates the adsorption of the adsorbates onto higher energy sites, resulting in the increase in the Langmuir constant for adsorption. The energy analysis reflects again that the mesopores in the CNFs promotes the transport of adsorbates during the VOCs adsorption process.

CONCLUSIONS

The present work has investigated that the contribution of porosity is an important factor determining the adsorption characteristics of CNFs in the vapor phase. The nitrogen physisorption technique indicated that the two kinds of CNFs possessed different pore structures including specific surface area and pore size distribution. Based on the analyses of the adsorption isotherms using Langmuir and DR equations, the existence of micropores in the CNFs act a major provider for VOCs adsorption, thus more micropore

fraction would promote a higher active surface occupied by the adsorbates. The main functionality of mesopores enables the adsorbates to get access to the inner and narrow micropores, which contain adsorptive sites having higher energy for adsorption. This argument has been supported by the larger values of both the equilibrium constant and the mean adsorption energy determined according to the Langmuir and the DR equations, respectively.

ACKNOWLEDGMENTS

The authors gratefully acknowledge the financial support from the National Science Council (NSC) and the Ministry of Education (MOE) in Taiwan, Republic of China (ROC).

REFERENCES

1. Iijima, S. (1991) Helical microtubules of graphitic carbon. *Nature*, 354: 56–58.
2. Li, D. and Xia, Y. (2004) Direct fabrication of composite and ceramic hollow nanofibers by electrospinning. *Nano Lett.*, 4: 933–938.
3. Li, Y.-H., Ding, J., Luan, Z., Di, Z., Zhu, Y., Xu, C., Wu, D., and Wei, B. (2003) Competitive adsorption of Pb^{2+}, Cu^{2+}, and Cd^{2+} ions from aqueous solutions by multiwalled carbon nanotubes. *Carbon*, 41: 2787–2792.
4. Shyu, Y.-M. and Hong, F.C.-N. (2001) The effects of pre-treatment and catalyst composition on growth of carbon nanofibers at low temperature. *Diamond Relat. Mater.*, 10: 1241–1245.
5. Ting, J.-M. and Huang, N.Z. (2001) Thickening of chemical vapor deposited carbon fiber. *Carbon*, 39: 835–839.
6. Ritschel, M., Uhlemann, M., Gutfleisch, O., Leonhardt, A., Graff, A., Täschner, C., and Fink, J. (2002) Hydrogen storage in different carbon nanostructures. *Appl. Phys. Lett.*, 80: 2985–2987.
7. Ma, R., Wei, B., Xu, C., Liang, J., and Wu, D. (2000) Catalytic growth of carbon nanofibers on a porous carbon nanotubes substrate. *J. Mater. Sci. Lett.*, 19: 1929–1931.
8. Li, N. and Martin, C.R. (2001) A high-rate, high-capacity, nanostructured Sn-based anode prepared using sol-gel template synthesis. *J. Electrochem. Soc.*, 148: A164–A170.
9. Wang, Y.-C., Leu, I.-C., and Hon, M.-H. (2002) Preparation of nanosized ZnO arrays by electrophoretic deposition. *Electrochem. Solid-State Lett.*, 5: C53–C55.
10. Schlottig, F., Textor, M., Georgi, U., and Roewer, G. (1999) Template synthesis of SiO_2 nanostructures. *J. Mater. Sci. Lett.*, 18: 599–601.
11. Hsieh, C.-T., Chen, J.-M., Kuo, R.-R., and Huang, Y.-H. (2004) Fabrication of well-aligned carbon nanofiber array and its gaseous-phase adsorption behavior. *Appl. Phys. Lett.*, 85: 1186–1188.
12. Eswaramoorthy, M., Sen, R., and Rao, C.N.R. (1999) A Study of micropores in single-walled carbon nanotubes by the adsorption of gases and vapors. *Chem. Phys. Lett.*, 304: 207–210.

13. Li, Y.-H., Wang, S., Wei, J., Zhang, X., Wei, J., Xu, C., Luan, Z., and Wu, D. (2003) Adsorption of fluoride from water by aligned carbon nanotubes. *Mater. Res. Bull.*, 38: 469–476.
14. Li, M.J., Bauschlicher, C.W., Jr., Ricca, A., and Meyyappan, M. (2003) Adsorption of 1,2-dichlorobenzene from water to carbon nanotubes. *Chem. Phys. Lett.*, 376: 761–766.
15. Peng, X., Li, Y., Luan, Z., Di, Z., Wang, H., Tian, B., and Jia, Z. (2003) CO_2 adsorption in single-walled carbon nanotubes. *Chem. Phys. Lett.*, 376: 154–158.
16. Lu, C., Chung, Y.-L., and Chang, K.-F. (2005) Adsorption of trihalomethanes from water with carbon nanotubes. *Water Res.*, 39: 1183–1189.
17. Stoeckli, H.F. (1990) Microporous carbons and their characterization: the present state of the art. *Carbon*, 28: 1–6.
18. Gregg, S.J. and Sing, K.S.W. (1982) *Adsorption, Surface Area and Porosity*; Academic Press: London.
19. Seaton, N.A., Walton, J.P.R., and Quirke, N. (1989) A new analysis method for the determination of the pore size distribution of porous carbons from nitrogen adsorption measurements. *Carbon*, 27: 853–861.
20. Ryu, Z., Zheng, J., and Wang, M. (1998) Porous structure of pan-based activated carbon fibers. *Carbon*, 36: 427–432.
21. Lin, Y.-R. and Teng, H. (2002) Mesoporous carbons from waste tire char and their application in wastewater discoloration. *Micropor. Mesopor. Mater.*, 54: 167–174.
22. Noll, K.E., Gournaris, V., and Hou, W.S. (1992) *Adsorption Technology for Air and Water Pollution Control*; Lewis Publishers: Chelsea, Michigan.
23. Avom, J., Mbadcam, J.K., Noubactep, C., and Germain, P. (1997) Adsorption of methylene blue from an aqueous solution onto activated carbons from palm-tree cobs. *Carbon*, 35: 365–369.
24. Teng, H. and Hsieh, C.-T. (1998) Influence of surface characteristics on liquid-phase adsorption of phenol by activated carbons prepared from bituminous coal. *Ind. Eng. Chem. Res.*, 37: 3618–3624.
25. Do, D.D. (1998) *Adsorption Analysis: Equilibria and Kinetics*; Imperial College Press: London.
26. Yang, O.-B., Kim, J.-C., and Kim, Y.-G. (1993) Use of activated carbon fiber for direct removal of iodine from acetic acid solution. *Ind. Eng. Chem. Res.*, 32: 1692–1697.
27. Barton, S.S. (1993) Adsorption from dilute, binary, aqueous solutions. *J. Colloid Interface Sci.*, 158: 64–70.
28. Hasany, S.M. and Saeed, M.M. (1992) A kinetic and thermodynamic study of silver sorption onto manganese dioxide from acid solutions. *Sep. Sci. Technol.*, 27: 1789–1800.
29. Hobson, J.P. (1969) Physical adsorption isotherms extending from ultrahigh vacuum to vapor pressure. *J. Phys. Chem.*, 73: 2720–2727.
30. Hiemenz, P.C. (1986) *Principles of Colloid and Surface Chemistry*; Marcel Dekker: New York.
31. Stoeckli, F. and Ballerini, L. (1991) Evolution of microporosity during activation of carbon. *Fuel*, 70: 557–559.
32. Lowell, S. and Shields, J.E. (1991) *Powder Surface Area and Porosity*; Chapman & Hall: London.